ACES Asian Chemical Editorial Society

DOI: 10.1002/asia.202001201

CHEMISTRY AN ASIAN JOURNAL Full Paper

Nature of Alkali- and Coinage-Metal Bonds versus Hydrogen Bonds

Olatz Larrañaga,[a] Ana Arrieta,[a] Célia Fonseca Guerra,[b, c] F. Matthias Bickelhaupt,*[b, d] and Abel de Cózar*[a, e]

Abstract: We have quantum chemically studied the structure and nature of alkali- and coinage-metal bonds (M-bonds) versus that of hydrogen bonds between A–M and B^- in archetypal $[A–M\cdots B]^-$ model systems (A, B=F, Cl and M=H, Li, Na, Cu, Ag, Au), using relativistic density functional theory at ZORA-BP86-D3/TZ2P. We find that coinage-metal bonds are stronger than alkali-metal bonds which are stronger than the corresponding hydrogen bonds. Our main purpose is to understand how and why the structure, stability and nature of such bonds are affected if the monovalent central atom H of hydrogen bonds is replaced by an isoelectronic alkali- or coinage-metal atom. To this end, we have analyzed the bonds between A–M and B^- using the activation strain model, quantitative Kohn-Sham molecular orbital (MO) theory, energy decomposition analysis (EDA), and Voronoi deformation density (VDD) analysis of the charge distribution.

1. Introduction

Intermolecular interactions have been an active topic in research for many years as they are cornerstones in supramolecular chemistry.[1] Although intermolecular interactions are generally weak compared to intramolecular interactions (as shown by the lower binding energies and large equilibrium distances of the formers), accumulation of many such weak interactions may lead to strong bonding in biomacromolecules such as DNA and proteins, thus pointing out its relevance also in biochemical processes.[2]

Among the various types of intermolecular interactions, the hydrogen bond (H-bond) has received particular attention.[3] Hydrogen bonding in complexes A–H···B are stabilizing interactions between a hydrogen-bond donor, i.e., a Lewis-acidic element-hydrogen (A–H) bond, and an electron-rich atom of the hydrogen bond acceptor (B), the electron-rich site of a Lewis base. Quantum-chemical bonding analyses have shown that the stabilization associated with the H-bond emerges not only from electrostatic interactions but also from substantial HOMO-LUMO orbital interactions that go with charge transfer from the lone-pair orbital of B to the σ^*_{AH} orbital of A–H.[4] Proceeding from the H-bond, one can replace the central hydrogen atom by a more electronegative halogen atom which leads us to the halogen bond (X-bond) in complexes A–X···B. This type of bond is relevant, e.g., in ligand-protein interactions.[5] In the framework of quantitative molecular orbital (MO) theory, the X-bond has been shown to possess a strong covalent character provided by HOMO-LUMO interactions that are very similar in nature to those occurring in H-bonds.[6] Valence bond (VB) theory studies have identified a number of X-bonds as charge-shift bonds.[7]

In this work, we wish to analyze the nature of a less explored, yet related type of intermolecular interaction: the metal bond (M-bond) in A–M···B:

$$A–M + B \rightarrow A–M\cdots B \quad (1)$$

Here, proceeding for example from an H-bond, the central hydrogen atom has been replaced by a more electropositive, monovalent metal atom M. The first prediction of an M-bond, namely, a lithium bond, was made by Kollman et al.[8] in 1970 and experimentally verified few years later.[9] Nevertheless, the Li-bond, and M-bond in general, are much less understood than the H- and X-bond.[10]

Herein, we aim to undertake a more systematic exploration of M-bonds, their structure and stability. Our purpose is in particular to understand their nature and bonding mechanism and to compare them with H- and X-bonds. To this end, we have quantum-chemically analyzed the structure and bonding of alkali- and coinage-metal bonds versus the hydrogen bonds between A–M and B^- in archetypal $[A–M\cdots B]^-$ model systems with A, B=F, Cl and M=H, Li, Na, Cu, Ag, Au, using relativistic density functional theory at ZORA-BP86-D3/TZ2P as implemented in the ADF program.[11] Our analyses are based on the activation strain model (ASM) of chemical reactivity[12] in

[a] Dr. O. Larrañaga, Prof. Dr. A. Arrieta, Dr. A. de Cózar
Departamento de Química Orgánica I, Facultad de Química, Universidad del País Vasco (UPV/EHU) and Donostia International Physics Center (DIPC)
P. K. 1072, 20018, San Sebastián-Donostia (Spain)
E-mail: abel.decozar@ehu.es

[b] Prof. Dr. C. Fonseca Guerra, Prof. Dr. F. M. Bickelhaupt
Department of Theoretical Chemistry, Amsterdam Center for Multiscale Modeling (ACMM), Vrije Universiteit Amsterdam, De Boelelaan 1083, 1081 HV Amsterdam (The Netherlands)
E-mail: f.m.bickelhaupt@vu.nl

[c] Prof. Dr. C. Fonseca Guerra
Leiden Institute of Chemistry, Leiden University, Einsteinweg 55, 2333 CC Leiden (The Netherlands)

[d] Prof. Dr. F. M. Bickelhaupt
Institute of Molecules and Materials, Radboud University, Heyendaalseweg 135, NL-6525 AJ Nijmegen (The Netherlands)

[e] Dr. A. de Cózar
IKERBASQUE, Basque Foundation for Science, Plaza Euskadi 5, 48009, Bilbao, Spain

Supporting information for this article is available on the WWW under https://doi.org/10.1002/asia.202001201

conjunction with quantitative Kohn-Sham molecular orbital (MO) theory and a canonical energy decomposition analysis (EDA).[13] Moreover, we have analyzed how the bonding affects the charge density distribution, using the Voronoi deformation density (VDD)[14] method.

2. Theoretical Methods

2.1. Computational details

All DFT calculations were carried out by using the Amsterdam Density Functional (ADF) program.[11] The molecular orbitals (MOs) were expanded in a large uncontracted set of Slater-type orbitals (STOs), TZ2P, which is of triple-ζ quality and has been augmented with two polarization function sets: 2p and 3d on hydrogen, 3d and 4f on fluorine and chlorine.

Equilibrium structures were obtained by optimizations using analytical gradient techniques.[11] Geometries and energies were calculated at the BP86 level of the generalized gradient approximation (GGA).[15] This level of theory has been shown of adequate accuracy for the treatment of similar three-atom systems such as Halogen bonding interactions (X-bond).[7] Relativistic effects were accounted for by using the zeroth-order regular approximation (ZORA).[16] Dispersion corrections were included by means of Grimme's D3 model.[17] All the minima were characterized by harmonic vibrational analysis, verifying that showed only positive definite Hessians. Thermal corrections computed at 298.15 K were found to have almost no influence on the observed trends, therefore, were not included in the discussion for clarity.

2.2. Activation Strain Analysis

The formation of the $D_{\infty h}$-symmetric $[A{-}M{\cdots}B]^-$ complex is associated with the occurrence of the new M···B bond between A–M and B^- and a simultaneous stretch of the already existing A–M bond in the neutral A–M molecule (for M=H, Li, see e.g. Ref. 18). This association process has been explored by analyzing the equilibrium geometry of $[A{-}M{\cdots}B]^-$ complex and a fictitious structure in which the A–M fragment remains as in an isolated A–M diatomic i.e. without stretching, while the M···B distance is as in the equilibrium geometry of the real $[A{-}M{\cdots}B]^-$.[19]

The complexation reactions were analyzed using the activation strain model (ASM) for the two above-mentioned situations.[12] Within this framework, the bond energy ΔE associated with forming the hydrogen bond or metal bond is decomposed according to Equation 2:

$$\Delta E = \Delta E_{strain} + \Delta E_{int} \quad (2)$$

Herein, ΔE_{strain} and ΔE_{int} correspond to the strain and interaction energy, respectively. The strain energy ΔE_{strain} is associated with the required energy to deform the reactants from their equilibrium geometry to the geometry they adopt in the hydrogen- or metal-bonded complex. This term depends on the extent of deformation, caused by the interaction, as well as the rigidity of the molecules involved in the association reaction. In general, the strain is positive (destabilizing). On the other hand, the interaction term ΔE_{int} depends on the electronic structure of the associating molecules and on how they approach each other. The interaction can be further analyzed within Kohn-Sham MO conceptual framework according to our canonical energy decomposition analysis (EDA)[13] as

$$\Delta E_{int} = \Delta V_{elstat} + \Delta E_{Pauli} + \Delta E_{oi} + \Delta E_{disp} \quad (3)$$

Herein, ΔV_{elstat} is the classical Coulombic interaction between the unperturbed charge distribution of each of the two reactants. The term ΔE_{Pauli} is the Pauli repulsions between occupied orbitals of the two fragments and is responsible for steric repulsion. The term ΔE_{oi} stands for the stabilizing orbital interaction energy, including charge transfer (such as HOMO-LUMO interactions). Finally, ΔE_{disp} constitutes a correction for dispersion interactions.

2.3. Voronoi Deformation Density (VDD) Analysis

The electron density distribution is analyzed using the Voronoi deformation density (VDD) method for computing atomic charges.[14] The VDD atomic charge (Q_A) is computed as the numerical integral of the deformation density in the volume of the Voronoi cell of atom A, that is, the compartment of space bounded by the bond midplanes on and perpendicular to all bond axes between nucleus A and its neighboring nuclei (Eq. 4).

$$Q_A = \int \left[\rho(r) - \sum\nolimits_B \rho_B(r)\right] dr \quad (4)$$

Here, $\rho(r)$ is the electronic density of the molecule and $\sum_B \rho_B(r)$ is the superposition of atomic densities $\rho_B(r)$ of a fictitious promolecule without chemical interactions where all atoms are considered neutral. Therefore, Q_A directly measures the charge that flows out of ($Q_A > 0$) or into ($Q_A < 0$) the Voronoi cell of atom A due to chemical interactions.

3. Results and Discussion

3.1. Trends in Structure and Stability

The results of our ZORA-BP86-D3/TZ2P calculations for the selected $[A{-}M{\cdots}B]^-$ (X=F, Cl; M=H, Li, Na, Cu, Ag, Au) complexes are collected in Table 1. Full structural details of the optimized structures and thermal corrections can be found in the Supporting Information.

All $[A{-}M{\cdots}B]^-$ complexes form spontaneously, without a barrier, on a single-well potential energy surface. Upon formation of the new B···M bond, the A–M bond of the original diatomic expands (vide infra), thus leading to a $D_{\infty h}$-symmetric

Table 1. Bond lengths d_{AM} (in Å), stretch of the A–M fragment Δd_{AM} (in Å), AM···B^- interaction energy decomposition analysis (in kcal mol^{-1}), VDD charge accumulation ΔQ_{AM} of fragment AM (in au), and overlap $\langle \sigma_{AM}{}^* | np_z(B^-) \rangle$ in optimized[a] and fictitious[b] $[A–M···B]^-$ complexes.

A–M	B^-	d_{AM}	Δd_{AM}	$d_{M\bullet\bullet\bullet B}$	ΔE	ΔE_{strain}	ΔE_{int}	ΔV_{elstat}	ΔE_{Pauli}	ΔE_{oi}				ΔE_{disp}	ΔQ_{AM}	$\langle \sigma_{AM}{}^* \| np_z(B^-) \rangle$
										total	σ	π	δ			
F–H	F^-	1.16	0.23	1.16	−53.2	19.8	−73.3	−76.3	68.1	−64.9	−58.0	−6.9	–	−0.2	−0.19	0.27
							(−37.8)	*(−72.9)*	*(83.1)*	*(−47.8)*	*(−41.5)*	*(−6.4)*		*(−0.1)*	*(−0.11)*	*(0.16)*
F–Li		1.70	0.12	1.70	−73.7	1.8	−75.6	−87.2	25.8	−14.2	−7.2	−7.5	–	−0.1	−0.06	0.11
							(−72.0)	*(−83.9)*	*(25.9)*	*(−13.9)*	*(−6.9)*	*(−6.9)*		*(−0.1)*	*(−0.06)*	*(0.10)*
F–Na		2.06	0.11	2.06	−65.8	1.0	−66.9	−77.4	20.9	−10.3	−5.3	−4.9	–	−0.1	−0.06	0.13
							(−64.8)	*(−75.6)*	*(21.0)*	*(−10.0)*	*(−5.2)*	*(−4.9)*		*(−0.1)*	*(−0.06)*	*(0.13)*
F–Cu		1.79	0.05	1.79	−96.9	0.6	−97.6	−124.3	71.6	−45.0	−32.7	−11.7	−0.6	−0.1	−0.20	0.26
							(−96.5)	*(−123.1)*	*(70.8)*	*(−44.2)*	*(−32.0)*	*(−11.6)*	*(−0.6)*	*(−0.1)*	*(−0.20)*	*(0.25)*
F–Ag		2.02	0.03	2.02	−81.8	0.1	−81.9	−105.7	67.6	−43.7	−33.9	−8.9	−0.9	−0.1	−0.23	0.24
							(−81.9)	*(−105.1)*	*(66.8)*	*(−43.3)*	*(−33.5)*	*(−8.9)*	*(−0.9)*	*(−0.1)*	*(−0.23)*	*(0.24)*
F–Au		1.99	0.04	1.99	−97.9	0.4	−98.3	−127.6	91.6	−62.3	−50.9	−10.4	−1.0	−0.1	−0.28	0.27
							(−97.6)	*(−126.8)*	*(90.4)*	*(−61.1)*	*(−49.7)*	*(−10.4)*	*(−1.0)*	*(−0.1)*	*(−0.27)*	*(0.27)*
F–H	Cl^-	1.01	0.08	1.86	−27.2	3.1	−30.4	−31.4	22.9	−21.5	−19.4	−2.1	–	−0.3	−0.11	0.36
							(−24.5)	*(−30.7)*	*(24.3)*	*(−17.8)*	*(−15.8)*	*(−2.0)*		*(−0.3)*	*(−0.09)*	*(0.34)*
F–Li		1.66	0.08	2.21	−49.2	1.1	−50.1	−55.6	16.0	−10.2	−6.0	−4.2	–	−0.2	−0.08	0.24
							(−48.4)	*(−53.9)*	*(15.9)*	*(−9.8)*	*(−5.8)*	*(−4.0)*		*(−0.2)*	*(−0.08)*	*(0.23)*
F–Na		2.04	0.09	2.55	−46.3	0.8	−47.1	−54.7	14.7	−6.7	−4.0	−2.7	–	−0.3	−0.06	0.25
							(−45.7)	*(−53.6)*	*(14.8)*	*(−6.5)*	*(−3.8)*	*(−2.7)*		*(−0.3)*	*(−0.06)*	*(0.25)*
F–Cu		1.80	0.06	2.10	−76.8	0.8	−77.7	−110.6	74.4	−41.4	−29.6	−11.2	−0.5	−0.2	−0.21	0.39
							(−76.2)	*(−109.1)*	*(74.0)*	*(−40.8)*	*(−29.1)*	*(−11.1)*	*(−0.5)*	*(−0.2)*	*(−0.20)*	*(0.39)*
F–Ag		2.03	0.08	2.33	−66.3	0.2	−66.5	−104.2	74.4	−36.5	−28.3	−7.7	−0.6	−0.2	−0.22	0.37
							(−66.0)	*(−103.2)*	*(73.5)*	*(−36.1)*	*(−27.9)*	*(−7.6)*	*(−0.6)*	*(−0.2)*	*(−0.22)*	*(0.37)*
F–Au		2.00	0.05	2.28	−81.8	0.7	−82.6	−131.3	107.2	−58.3	−47.0	−10.6	−0.7	−0.2	−0.27	0.38
							(−81.5)	*(−129.6)*	*(105.8)*	*(−57.2)*	*(−45.9)*	*(−10.6)*	*(−0.8)*	*(−0.2)*	*(−0.26)*	*(0.38)*
Cl–H	Cl^-	1.59	0.30	1.59	−29.9	17.5	−48.0	−45.5	65.0	−67.1	−62.4	−4.6	–	−0.5	−0.25	0.34
							(−17.3)	*(−45.5)*	*(77.8)*	*(−49.2)*	*(−44.3)*	*(−4.9)*		*(−0.3)*	*(−0.15)*	*(0.21)*
Cl–Li		2.17	0.14	2.17	−56.9	1.6	−58.5	−62.8	18.2	−13.5	−7.8	−5.7	–	−0.4	−0.10	0.26
							(−55.6)	*(−60.2)*	*(18.0)*	*(−13.0)*	*(−7.4)*	*(−5.6)*		*(−0.4)*	*(−0.09)*	*(0.25)*
Cl–Na		2.52	0.13	2.52	−51.8	1.1	−52.9	−60.6	16.6	−8.6	−5.1	−3.4	–	−0.4	−0.17	0.26
							(−50.8)	*(−58.9)*	*(16.7)*	*(−8.2)*	*(−4.9)*	*(−3.4)*		*(−0.4)*	*(−0.07)*	*(0.26)*
Cl–Cu		2.11	0.07	2.11	−76.7	0.8	−77.5	−110.9	77.2	−43.5	−31.1	−12.1	−0.4	−0.4	−0.22	0.38
							(−42.8)	*(−109.6)*	*(76.7)*	*(−42.8)*	*(−30.3)*	*(−12.1)*	*(−0.4)*	*(−0.4)*	*(−0.22)*	*(0.38)*
Cl–Ag		2.35	0.05	2.35	−66.9	0.3	−67.3	−102.1	73.0	−37.8	−28.9	−8.3	−0.5	−0.4	−0.23	0.36
							(−66.7)	*(−101.3)*	*(72.3)*	*(−37.3)*	*(−28.4)*	*(−8.4)*	*(−0.5)*	*(−0.4)*	*(−0.27)*	*(0.36)*
Cl–Au		2.31	0.07	2.31	−77.5	0.9	−78.4	−125.5	105.8	−58.3	−47.0	−10.7	−0.6	−0.4	−0.29	0.37
							(−76.7)	*(−124.2)*	*(104.7)*	*(−57.0)*	*(−45.5)*	*(−10.8)*	*(−0.6)*	*(−0.4)*	*(−0.28)*	*(0.37)*

[a] Computed at ZORA-BP86-D3/TZ2P. [b] Results obtained for a fictitious $[A–M···B]^-$ structure in which the A–M fragment is in the equilibrium geometry of an isolated diatomic molecule ($\Delta d_{AM} = 0.00$) while the M···B distance is as in the equilibrium geometry of the real $[A–M···B]^-$ complex in italics and parentheses.

ACES Asian Chemical Editorial Society
CHEMISTRY AN ASIAN JOURNAL
Full Paper

equilibrium geometry. The following main trends emerge from our computations: In the first place, coinage metal bonds are stronger than the corresponding alkali metal bonds and the latter are stronger than hydrogen bonds. For example, the F–M $+F^-$ bond energy ΔE amounts to about −82, −66 and −53 kcal mol^{-1} for M=Ag, Na and H, respectively (see Table 1).

Secondly, the metal bonds are consistently longer than the corresponding hydrogen bonds, by up to ca 1 Å. For example, $d_{M\bullet\bullet\bullet B}$ in $[F–M\cdots F]^-$ is 2.02, 2.06 and 1.16 Å, for M=Ag, Na and H, respectively (see Table 1).

Thirdly, the A–M stretch Δd_{AM} tends to be larger in most cases for hydrogen than for metal bonds (see Table 1). For example, Δd_{AM} in $[F–M\cdots F]^-$ is 0.03, 0.11 and 0.23 Å, again for M=Ag, Na and H, respectively (see Table 1). As we will see later on, the A–M bond stretching is a consequence of charge transfer from the lone-pair orbital of B^- to the antibonding σ^*_{AM} orbital of A–M, similar to the situation for hydrogen bonds.[4]

Lastly, both M- as well as H-bonded complexes of A–M involving the base B^-=F^- are more stable than the corresponding ones involving the base B^-=Cl^-. This is in line with the higher proton and alkali cation affinities of the fluoride compared to the chloride anion.[20] For example, the complexation energy ΔE of FLi, FNa and FH with F^- is −73.7, −65.8 and −53.2 kcal mol^{-1} which is significantly more stabilizing that the corresponding ΔE of −49.2, −46.3 and −27.2 kcal mol^{-1} for complexation of the same series of diatomics with Cl^- (see Table 1).

3.2. Nature of the Metal Bond and Trends in Bonding

Our quantitative MO bonding analyses reveal that all metal-bonds, coinage and alkali, have in essence a similar bonding mechanism, with both electrostatic and covalent interactions, as the corresponding hydrogen bonds. The metal bonds, however, mostly go with a significantly stronger electrostatic attraction than the hydrogen bonds, in line with the more pronounced polarization in the $A^{\delta-}–M^{\delta+}$ than $A^{\delta-}–H^{\delta+}$ bond (see Q_M in Table 2) and because of the higher nuclear charge of the metal atoms around which the B^- lone pair extends. This is an important reason why all metal bonds, especially coinage-metal bonds, are stronger than H bonds. Dispersion interactions are essentially negligible with values of half a kcal mol^{-1} at most.

Furthermore, in $[A–M\cdots B]^-$, the np_z lone-pair of the base B^- engages into a HOMO-LUMO interaction with the σ_{AM}* of the A–M diatomic (see Figure 1). This leads to a significant covalent component, i.e., orbital interaction ΔE_{oi}, in the bonding

Table 2. Bond length d_{AM} (in Å), homolytic bond dissociation energies BDE (in kcal mol^{-1}), VDD charge Q_M of atom M (in au), frontier orbital energies ε (in eV) and overlaps of A–M molecules.[a]

					character σ_{AM}*[b]		$\varepsilon(\sigma_{AM}$*$)$[c]		$<np_\sigma(A)\,\vert\,ns(M)>$[c]	
AM	d_{AM}	BDE	Q_M	$\varepsilon(\sigma_{AM})$	%np_σ(A)	%ns(M)	eq	eq + 0.5 Å	eq	eq + 0.5 Å
FH	0.93	150.5	0.20	−13.55	4	48	−0.74	−4.73	0.38	0.27
FLi	1.58	145.7	0.51	−6.45	0	82	−1.31	−1.90	0.10	0.12
FNa	1.95	120.4	0.60	−5.27	2	82	−1.74	−2.25	0.10	0.11
FCu	1.74	106.5	0.37	−6.36	10	65	−4.36	−5.16	0.18	0.15
FAg	1.99	89.3	0.42	−6.91	10	75	−4.25	−4.95	0.16	0.14
FAu	1.95	80.5	0.28	−7.32	17	61	−5.24	−6.17	0.17	0.13
ClH	1.29	110.4	0.10	−11.85	22	72	−1.09	−4.52	0.48	0.32
ClLi	2.03	112.1	0.47	−6.53	0	76	−1.81	−2.32	0.22	0.20
ClNa	2.38	95.5	0.58	−5.74	3	79	−2.02	−2.47	0.19	0.16
ClCu	2.04	87.6	0.29	−6.54	13	60	−4.18	−4.96	0.29	0.22
ClAg	2.30	73.8	0.36	−7.11	13	68	−4.17	−4.87	0.26	0.19
ClAu	2.23	70.0	0.21	−7.40	22	55	−4.91	−5.82	0.28	0.20

[a] Computed at ZORA-BP86-D3/TZ2P. [b] Gross Mulliken contribution (in %) to σ_{AM}*. [c] Evaluated at the equilibrium A–B bond length of AM (d_{AM}) and at an A–M distance that has been stretched from the equilibrium geometry by 0.5 Å (d_{AM} + 0.5 Å).

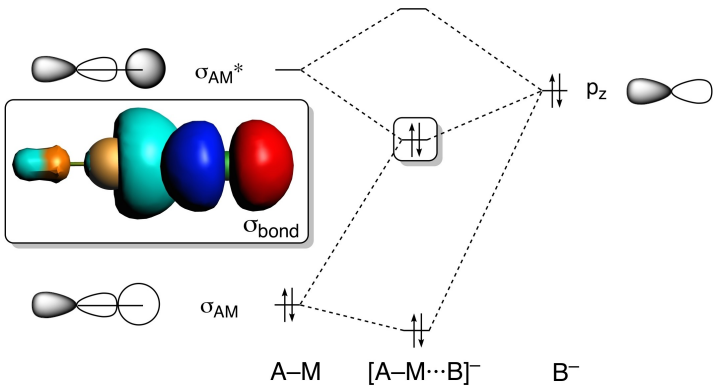

Figure 1. Schematic orbital-interaction diagram for $[A–M\cdots B]^-$ complexes as they emerge from our quantitative MO analyses for M=H, Li, Na, Cu, Ag and Au, computed at ZORA-BP86-D3/TZ2P, with a 3D plot of the bonding σ_{AM}* + $np_z(B^-)$ combination of $[F–Cu\cdots F]^-$.

mechanism which reinforces the electrostatic attraction ΔV_{elstat} between the polarized $F^{\delta-}$–$M^{\delta+}$ bond and the negatively charged Lewis base F^- (see Table 1). The percentage contribution of the covalent component (ΔE_{oi}) to the total bonding forces ($\Delta V_{elstat} + \Delta E_{oi} + \Delta E_{disp}$) is, however, smaller in the metal bonds than in the corresponding hydrogen bonds (vide infra). For example, in the strongest coinage-metal complex, [F–Au···F]$^-$, the gold-bond with an overall bond energy ΔE_{int} of -98.3 kcal mol^{-1} receives -62.3 kcal mol^{-1} of stabilization from orbital interaction ΔE_{oi}, and -50.9 kcal mol^{-1} indeed stem from the σ-orbital interactions ΔE_{σ}. Although this is less than the electrostatic attraction of -127.6 kcal mol^{-1}, it is still about half the magnitude of the latter and thus of crucial importance for the stability and the nature of the bond. For comparison, in the corresponding hydrogen-bonded complex, [F–H···F]$^-$, the overall bond energy ΔE_{int} of -73.3 kcal mol^{-1} receives -64.9 kcal mol^{-1} of stabilization from orbital interaction ΔE_{oi} (-58.0 kcal mol^{-1} of which are σ-orbital interactions) and -76.3 kcal mol^{-1} from electrostatic attraction ΔV_{elstat}.

Next, after characterizing the nature of alkali- and coinage-metal bonds, we examine in more detail the computed trend in bond strengths: why does the bond strength ΔE weaken along coinage-metal bonds, alkali-metal bonds and hydrogen bonds? Our analyses show that three phenomena in the bonding mechanism contribute significantly to this trend (see Table 1): (i) more stabilizing electrostatic attraction in the case of the metal bonds due to, among others, the aforementioned higher polarization in the $A^{\delta-}$–$M^{\delta+}$ bond and, especially for the coinage-metal bonds, a higher nuclear charge at M;[8,21,22] (ii) more stabilizing orbital interactions in the coinage than in the alkali-metal bonds due to a lower orbital energy of the σ^*_{AM} LUMO, and thus stronger HOMO-LUMO interaction with the Lewis base, in the case of the former; and (iii) less Pauli repulsion for the alkali-metal bonds in which the occupied σ_{AM} bond orbital is mainly localized on A leading to little 2-orbital-4-electron repulsion with the $np_z(B^-)$ HOMO (overlap not shown in Table 1).

The more stabilizing orbital interactions in the coinage-metal bonds than in the alkali-metal bonds are a consequence of the lower energy of the σ_{AM}* and the larger HOMO-LUMO overlap in the former. This LUMO emerges mainly from the antibonding combination of the np_{σ}(A) and the ns(M), where the ns(M) of the significantly less electropositive coinage-metal atoms is already lower in energy than that of the more electropositive alkali-metal atoms, and therefore, closer in energy to $np_z(F^-)$, yielding a smaller, i.e., more favorable orbital-energy gap. For example, in the strongest alkali complex [F–Li···F]$^-$ ($\Delta E = -73.7$ kcal mol^{-1} see Table 1), the poor HOMO-LUMO overlap ($\langle \sigma_{FLi}{}^* | np_z(F^-) \rangle = 0.11$) implies a low orbital interaction (ΔE_{oi}) of -14.2 kcal mol^{-1}; whereas, in the strongest coinage complex [F–Au···F]$^-$ ($\Delta E = -97.9$ kcal mol^{-1}), the HOMO-LUMO overlap is twice as large as in the lithium case ($\langle \sigma_{FAu}{}^* | np_z(F^-) \rangle = 0.27$), thus exhibiting stronger stabilization orbital interaction ($\Delta E_{oi} = -62.3$ kcal mol^{-1}).

The energetic difference in bond strength between coinage and alkali bonds is, as already alluded to above, partially compensated by the lower Pauli repulsion of highly polarized alkali bond ($\Delta E_{Pauli} = 25.8$ kcal mol^{-1} for [F–Li···F]$^-$ compared to $\Delta E_{Pauli} = 91.6$ kcal mol^{-1} for [F–Au···F]$^-$ see Table 1) in which the A–M HOMO σ_{FAu} has little amplitude on the metal (see Figure S1 in the Supporting Information).

3.3. A–H versus A–M stretching

Finally, we notice that hydrogen bonds [A–H···B]$^-$ go with a substantially larger A–H expansion than the corresponding A–M expansion in metal bonds [A–M···B]$^-$, despite the higher rigidity of the element-hydrogen bond than the element-metal bond in the A–H versus A–M molecule. For example, the diatomic F–H, with a sizeable homolytic bond dissociation energy (BDE) of ca 150 kcal mol^{-1} (see Table 2), elongates 0.23 Å due to the complexation process (see Table 1) whereas the much weaker F–Au bond (BDE of 80.5 kcal mol^{-1}) elongates by only 0.04 Å.

Our analyses reveal that the more substantial elongation of the A–H bond in hydrogen bonds is ultimately caused to the difference in bond-length dependence of the $\langle np_{\sigma}(A) | ns(M) \rangle$ overlap for M=hydrogen or metal in the A–M molecule. This difference is behind an important phenomenon, namely, that the orbital energy of the σ^*_{AH} LUMO drops much faster upon A–H expansion than the σ^*_{AM} LUMO does upon A–M expansion and consequently leads to a larger gain in stabilizing orbital interaction upon A–H expansion in hydrogen bonds. For example, if we elongate the F–H bond of the hydrogen fluoride molecule from its equilibrium geometry by 0.5 Å, the $\langle 2p_{\sigma}(F) | 1s(H) \rangle$ orbital overlap significantly decreases from 0.38 to 0.27 and the orbital energy of the σ_{FH}* LUMO drops significantly, from -0.74 to -4.74 eV (see Table 2), and becomes a better electron accepting LUMO for the HOMO of the F^- Lewis base in [F–H···F]$^-$. In line with this, in [F–H···F]$^-$, the stabilizing orbital interactions ΔE_{oi} are enhanced from -47.8 to -64.9 kcal mol^{-1}, if we go from the fictitious situation in which the F–H molecule preserves its own, shorter equilibrium bond distance of 0.93 Å of (see Table 1). This larger gain in orbital interactions drives the A–H expansion and compensates the associated raise in strain energy.

Ultimately, this behavior could be traced to the more compact nature of the hydrogen 1s AO if compared to the metal ns AOs (see Figure 2). In the A–H molecule, the hydrogen 1s AO engages into a textbook overlap with the A np_{σ} AO, i.e., an overlap of significant magnitude which quickly drops, as the A–H bond expands and, thus, causes the np_{σ}(A)–1 s combination which mainly constitutes the σ^*_{AH} to lose its A–H antibonding overlap quickly and thus drop in energy rapidly. This can be seen in Figure 2A which shows the on-scale 3D representation of the overlapping np_{σ}(F) and 1 s(H) atomic orbitals.

At variance, in the A–M molecules, the A np_{σ} AO achieves only a moderate overlap with the significantly more diffuse metal ns AO, and this overlap also changes less upon bond elongation than in the case of A–H. This situation arises in particular for the A–M systems involving alkali-metal atoms (see Figure 2). Thus, the A–M antibonding character of the σ^*_{AM}

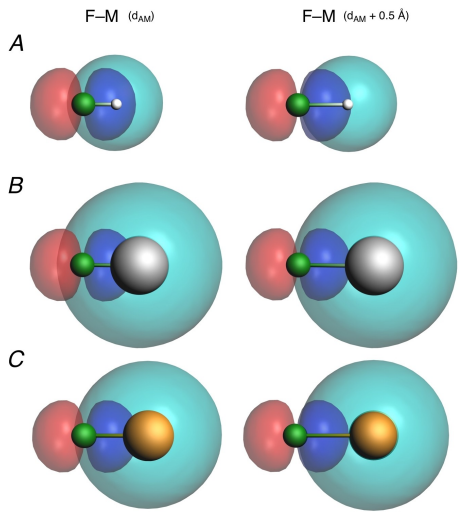

Figure 2. 3D plot of $2p_\sigma(F^-)$ and n*s*(M) orbitals in A–M molecules at equilibrium distance (left) and stretched by +0.5 Å (right) for (A) M=H, (B) M=Li and (C) M=Cu at isosurface value of 0.03. $2p_\sigma(F^-)$ orbitals are represented in blue & red and n*s*(M) orbitals are in turquoise for clarity.

weakens more moderately and the orbital energy of this LUMO goes down to a lesser extent than in the case of the σ^*_{AH} LUMO. For example, if we elongate the F–Li bond of the lithium fluoride molecule from its equilibrium geometry by 0.5 Å, the $\langle 2p_\sigma(F)|2s(Li)\rangle$ orbital overlap hardly changes and in fact even slightly increases, from 0.10 to 0.12 (see Table 2). The slight increase, instead of decrease, is related to the very diffuse nature of the Li 2 *s* AO which ranges across the F $2p_\sigma$ nodal surface; this can be clearly seen in Figure 2B. Thus, F–Li elongation initially improves the overlap because unfavorable cancelation effects disappear (ultimately, if one would contribute to elongate the F–Li bond, the overlap of course decreases and goes towards zero). Altogether, the F–Li elongation by 0.5 Å has little effect on the orbital energy of the σ_{FH}* LUMO which goes from −1.31 to −1.90 eV (see Table 2). As a consequence, in metal bonds [A–M···B]$^-$, the orbital interactions ΔE_{oi} in general hardly benefit from A–M elongation, by up to ca 1 kcal mol^{-1} only (see Table 1).

4. Conclusions

Coinage-metal bonds and, to a lesser extent, alkali-metal bonds in [A–M···B]$^-$ model complexes are stronger than the corresponding hydrogen bonds in [A–H···B]$^-$. The metal-bonds have a substantial covalent component provided by the HOMO-LUMO interaction of the occupied np_z of B$^-$ and the empty A–M antibonding σ^*_{AM} that reinforces electrostatic attraction between the polarized metal-bond donor $A^{\delta-}$–$M^{\delta+}$ and the anionic Lewis base B$^-$, similar to the bonding mechanism in hydrogen bonds, although covalency is more important in the latter. This follows from our quantitative MO bonding analyses of [A–M···B]$^-$ model complexes (M=H, Li, Na, Cu, Ag, Au; A, B=F, Cl) based on dispersion-corrected relativistic density functional theory.

The trend in bond strengths originates from two phenomena: (i) the metal bonds have a stronger electrostatic attraction than the hydrogen bonds because of a more pronounced polarization in the $A^{\delta-}$–$M^{\delta+}$ bond in the former; and (ii) coinage-metal bonds are stronger than alkali-metal bonds due to more stabilizing orbital interactions. This latter trend is the result of a lower, more favorable orbital energy of the σ^*_{AM} LUMO and a somewhat better more compact nature on M, leading to better overlap with the B$^-$ np_z HOMO, when M goes from the alkali metals to the somewhat more electronegative and effectively smaller coinage metals.

Finally, hydrogen bonds [A–H···B]$^-$ go with a substantially larger A–H expansion than the corresponding A–M expansion in metal bonds [A–M···B]$^-$, despite the higher rigidity of the element-hydrogen than element-metal bond in the AH versus AM molecule. The reason for this is that the orbital energy of the σ^*_{AH} LUMO drops much faster upon A–H expansion than the σ^*_{AM} LUMO does upon A–M expansion and consequently leads to a larger gain in stabilizing orbital interaction upon A–H expansion in hydrogen bonds. This phenomenon could be traced to the difference in compactness of hydrogen (more compact) and, e.g., an alkali metal atom (more diffuse).

Acknowledgements

O.L. gratefully acknowledges the UPV/EHU for her postdoctoral grant. This work was supported by funding provided by the Spanish Ministry of Economy and Competitiveness (MINECO CTQ2013-45415P and CTQ2016-80375P), the Gobierno Vasco-Eusko Jaurlaritza (Grant IT673-13) and the Netherlands Organization for Scientific Research (NWO). We also thank SURFsara for the support in using the Lisa Computer Cluster, and DIPC and SGI-IZO-SGIker (UPV/EHU) for generous allocation of computational resources.

Conflict of Interest

The authors declare no conflict of interest.

Keywords: Activation Strain Model · Bond theory · DFT calculations · Hydrogen bonding · Metal bonding

[1] a) J.-M. Lehn, *Supramolecular Chemistry. Concepts and Perspectives*, VCH, Weinheim, **1995**; b) K. Müller-Dethlefs, P. Hobza, *Chem. Rev.* **2000**, *100*, 143–168; c) G. A. Jeffrey, *An Introduction to hydrogen Bonding*, Oxford University Press: New York, **1997**.
[2] a) P. Hobza, J. Sponer, *Chem. Rev.* **1999**, *99*, 3247–3276; b) J. L. Cifelli, C. C. Capule, J. Yang, *ACS Chem. Neurosci.* **2019**, *10*, 991–995.
[3] a) H. Umeyama, K. Morokuma, *J. Am. Chem. Soc.* **1977**, *99*, 1316–1332; b) G. R. Desiraju, T. Steiner, *The Weak Hydrogen Bond in structural Chemistry and Biology*, Oxford University Press Inc.: New York, **1999**; c) S. J. Grabowski, *Chem. Rev.* **2011**, *111*, 2597–2625; d) S. C. C. van der Lubbe, C. Fonseca Guerra, *Chem. Asian J.* **2019**, *14*, 2760–2769; e) S. C. C. van der Lubbe, F. Zaccaria, X. Sun, C. Fonseca Guerra, *J. Am. Chem. Soc.* **2019**, *141*, 4878–4885; f) S. C. C. van der Lubbe, C. Fonseca Guerra, *Chem. Eur. J.* **2017**, *23*, 10249–10253.

[4] C. Fonseca Guerra, F. M. Bickelhaupt, J. G. Snijders, E. J. Baerends, *Chem. Eur. J.* **1999**, *5*, 3581–3594.
[5] a) A. R. Voth, P. Khuu, K. Oishi, P. S. Ho, *Nat. Chem.* **2009**, *1*, 74–79; b) C.-Z. Liu, S. Koppireddi, H. Wang, D.-W. Zhang, Z.-T. Li, *Angew. Chem. Int. Ed.* **2018**, *58*, 226–230; *Angew. Chem.* **2018**, *130*, 1–6; c) E. Margiotta, S. C. C. van der Lubbe, L. Santos, G. Paragi, S. Moro, F. M. Bickelhaupt, C Fonseca Guerra, *J. Chem. Inf. Model.* **2020**, *60*, 1317–1328; d) G. Cavallo, P. Metrangolo, R. Milani, T. Pilati, A. Priimagi, G. Resnati, G. Terraneo *Chem. Rev.* **2016**, *116*, 2478–2601.
[6] a) L. P. Wolters, F. M. Bickelhaupt, *ChemistryOpen* **2012**, *1*, 96–105; b) L. P. Wolters, P. Schyman, M. J. Pavan, W. L. Jorgensen, F. M. Bickelhaupt, S. Kozuch, *WIREs Comput. Mol. Sci.* **2014**, *14*, 523–540; c) F. M. Bickelhaupt, E. J. Baerends, N. M. M. Nibbering, *Chem. Eur. J.* **1996**, *2*, 196–207.
[7] C. Wang, D. Danovich, Y. Mo, S. Saik *J. Theory. Comput.* **2014**, *10*, 3726–3737.
[8] P. A. Kollman, J. F. Liebmanm, L. C. Allen, *J. Am. Chem. Soc.* **1970**, *92*, 1142–1150.
[9] B. S. Ault, G. C. Pimentel, *J. Phys. Chem.* **1975**, *79*, 621–626.
[10] A. B. Sannigrahi, T. Kar, B. G. Nigoyi, P. Hobza, P. v. R. Schleyer, *Chem. Rev.* **1990**, *90*, 1061–1076.
[11] S. C. M. ADF2017.110 Theoretical Chemistry, Vrije Universiteit Amsterdam, **2017**. See: www.scm.com.
[12] a) F. M. Bickelhaupt, *J. Comput. Chem.* **1999**, *20*, 114–128; b) I. Fernandez, F. M. Bickelhaupt, *Chem. Soc. Rev.* **2014**, *43*, 4953–4967; c) L. P. Wolters, F. M. Bickelhaupt, *WIREs Comput. Mol. Sci.* **2015**, *5*, 324–343; d) F. M. Bickelhaupt, K. N. Houk, *Angew. Chem. Int. Ed.* **2017**, *56*, 10070–10086; *Angew. Chem.* **2017**, *129*, 10204–10221.
[13] a) F. M. Bickelhaupt, E. J. Baerends *Reviews in Computational Chemistry, Vol. 15*; K. B. Lipkowitz, D. B. Boyd, Eds.; Wiley-VCH: New York, **2000**, pp. 1–86; b) M. Lein, G. Frenking, *Theory and Applications of Computational Chemistry. The First 40 Years*; C. E. Dykstra, G. Frenking, K. S. Kim, G. E. Scuseria, Eds.; Elsevier: Amsterdam, **2005**.
[14] C. Fonseca Guerra, J. W. Handgraaf, E. J. Baerends, F. M. Bickelhaupt, *J. Comput. Chem.* **2004** *25*, 189–210.
[15] a) A. D. Becke, *Phys. Rev. A* **1988**, *38*, 3098–3100; b) J. P. Perdew, *Phys. Rev. B* **1986**, *33*, 8822–8824.
[16] E. van Lenthe, E. J. Baerends, J. G. Snijders, *J. Chem. Phys.* **1994**, *101*, 9783.
[17] S. Grimme, J. Antony, S. Ehrlich, H. J. Krieg *J. Chem. Phys.* **2010**, *132*, 154104.
[18] S. A. C. McDowell, J. A. S. S. Hill, *J. Chem. Phys.* **2011**, *135*, 164303.
[19] A. P. Bento, F. M. Bickelhaupt, *J. Org. Chem.* **2007**, *73*, 7290–7299.
[20] a) Z. Boughala, C. Fonseca Guerra, F. M. Bickelhaupt, *Chem. Asian J.* **2017**, *12*, 2604–2611; b) Z. Boughala, C. Fonseca Guerra, F. M. Bickelhaupt, *Cation Affinities throughout The Periodic Table in Advances in Inorganic Chemistry Vol. 73;* R. van Eldik, R. Puchta, Eds.; Academic Press: San Diego, **2019**; Chapter 6.
[21] P. Lipkowski, S. J. Grabowski, *Chem. Phys. Lett.* **2014**, *591*, 113–118.
[22] S. Scheiner in *Lithium Chemistry, Theoretical and Experimental Overview*; A. M. Sapse, P. v. R. Schleyer, Eds.; Willey: New York, **1995**; p. 67–87.

Manuscript received: October 13, 2020
Revised manuscript received: December 28, 2020
Accepted manuscript online: December 29, 2020
Version of record online: January 14, 2021